vidin, Pierce) was used in place of conventional avidin in all measurements. Streptavidin from *Streptomyces avidinii*, derivatized agarose beads, and biotin-BSA were purchased from Sigma.
7. This equation is not valid for all ligand-receptor systems. Because of the complexity of the pair potential, there is no simple relation between unbinding force and binding energy for the general case. A more appropriate expression is $F_u = \Delta H^*/r_{eff}$, where ΔH^* is the enthalpy of activation.
8. This approximation is based on the assumption that the effective spring constant of the system is significantly smaller than the spring constant of the avidin-biotin complex. Strictly speaking, separation occurs when the gradient of the external force exceeds the second derivative of the pair potential.
9. N. M. Green, *Biochem. J.* **101**, 774 (1966).
10. P. Sheterline and J. C. Sparrow, Eds., *Actin* (Academic Press, London, 1994), vol. 1.
11. The force required to rupture a single actin filament was measured with microneedles to be approximately 110 pN [A. Kishino and T. Yanagida, *Nature* **334**, 74 (1988)]. A derivation of r_{eff} requires knowledge of the enthalpy of activation. The enthalpy of the actin monomer-monomer bond is endothermic with a value of about 15 kcal/mol. Assuming an upper limit of 20 kcal/mol for the enthalpy of activation, the enthalpy of activation for the backward reaction (monomer-monomer dissociation) is estimated to be 5 kcal/mol.
12. On the basis of an elastic model, the microscopic elastic constant of the monomer-monomer bond was calculated from the bending elastic modules [F. Oosawa, *Biorheology* **14**, 11 (1977)]. Assuming an elastic constant of 2 N/m, Hooke's Law yields a r_{eff} value of 0.5 Å.
13. W. Kabsch, H. G. Mannherz, D. Suck, E. F. Pai, K. C. Holmes, *Nature* **347**, 37 (1990); K. C. Holmes, D. Popp, W. Gebhard, W. Kabsch, *ibid.*, p. 44.
14. There is as much as 20% variability among the different methods used in the calibration of cantilevers [V. T. Moy, E.-L. Florin, H. E. Gaub, unpublished results; J. P. Cleveland, S. Manne, D. Bocek, P. K. Hansma, *Rev. Sci. Instrum.* **64**, 403 (1993); J. L. Hutter and J. Bechhoefer, *ibid.*, p. 1868; T. J. Senden and W. A. Ducker, *Langmuir* **10**, 1003 (1994)]. The values reported here are based on cantilevers calibrated with a macroscopic reference lever in a method that does not depend on the high-frequency response of the cantilever.
15. P. C. Weber, J. J. Wendololoski, M. W. Pantoliano, F. R. Salemme, *J. Am. Chem. Soc.* **114**, 3197 (1992).
16. This work was supported by the Deutsche Forschungsgemeinschaft. We are grateful to S. Kilger and G. Cevc for their assistance in the titration microcalorimetry measurements; to E. Sackmann, H. M. McConnell, and J. Brauman for inspiring discussions; and to Digital Instruments for technical support.

25 May 1994; accepted 2 September 1994

Partial Control of an Ion-Molecule Reaction by Selection of the Internal Motion of the Polyatomic Reagent Ion

Robert D. Guettler, Glenn C. Jones Jr., Lynmarie A. Posey,* Richard N. Zare†

The ion-molecule reaction $NH_3^+ + ND_3$ has been studied at various collision energies (1 to 5 electron volts in the center of mass) with preparation of the NH_3^+ reagent in two nearly isoenergetic vibrational states. One state corresponds to pure out-of-plane bending of the planar NH_3^+ ion (0.60 electron volts), whereas the other state is a combination of in-plane and out-of-plane motion (0.63 electron volts). The product branching ratios differ markedly for these two vibrational-state preparations. The differences in reactivity suggest that the in-plane totally symmetric stretching mode is essentially inactive in controlling the branching ratio of this reaction.

Most chemical reactions are statistical in nature, and their course cannot be controlled by the excitation of different vibrational motions of the reactants, but outstanding exceptions are known to occur for small reaction systems (*1*, *2*). For example, H (*3*–*6*) or Cl (*7*) can selectively abstract the H or D atom from HOD depending on the vibrational excitation of the HOD reagent. The results for the H + HOD and Cl + HOD reactions conform to intuition in that the bond being stretched reacts; that is, motion along the reaction coordinate promotes reaction (*8*).

In the case of more complex reactants, almost no experimental information exists on the role of reagent internal motion in directing the outcome of a reactive encounter (*9*, *10*), although some theoretical calculations (*11*, *12*) suggest that such effects may be important. We present here a study of the ion-molecule reaction

$$NH_3^+(\nu_1,\nu_2) + ND_3 \rightarrow NH_3D^+ + ND_2 \quad \text{(deuterium abstraction)} \quad (1a)$$

$$\rightarrow NH_3 + ND_3^+ \quad \text{(charge transfer)} \quad (1b)$$

$$\rightarrow NH_2 + ND_3H^+ \quad \text{(proton transfer)} \quad (1c)$$

in which the NH_3^+ reagent ion is prepared in nearly isoenergetic internal states having different vibrational motions. The NH_4^+ isotopomer channels (Eq. 1, a and c) have an exothermicity of ~0.9 eV (*13*), whereas the charge transfer product channel (Eq. 1b) is nearly thermoneutral. The branching ratio among these three product channels can be partially controlled by the choice of reagent ion internal motion.

The NH_3^+ ion is an ideal reactant for state-selected studies because multiphoton ionization can be used to prepare the ion with a wide range of controlled vibrational excitation (*14*, *15*). A resonant two-photon excitation from the pyramidal ground state to the planar $\tilde{B}$ or $\tilde{C}'$ Rydberg state of the ammonia molecule selects an intermediate vibrational state. The large change in geometry that results from these transitions allows excitation to be placed into two vibrational modes of the molecule. The pyramidal-to-planar change in geometry allows access to an extended progression of out-of-plane totally symmetric bending vibrations (*16*), referred to here as the umbrella bending mode (ν_2) (Fig. 1A). In addition, a slight lengthening of the N–H bond can excite the in-plane totally symmetric stretch vibration (*15*, *17*), referred to here as the breathing mode (ν_1) (Fig.

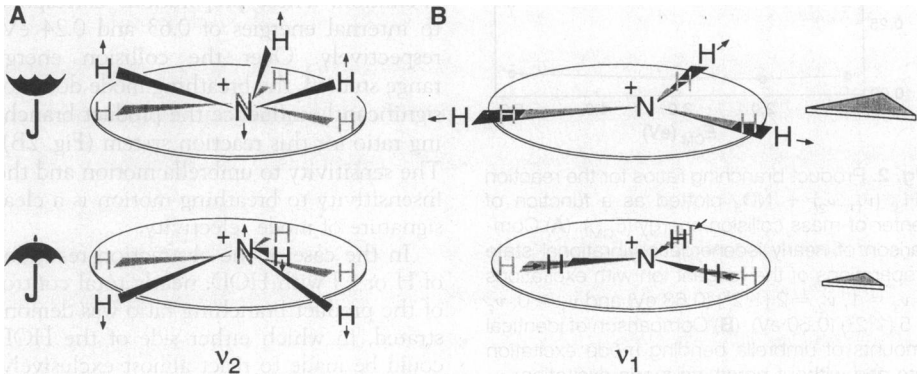

Fig. 1. Two of the six vibrational modes of the planar NH_3^+ ion: (**A**) the umbrella bending mode (ν_2) (out-of-plane totally symmetric bending mode) and (**B**) the breathing mode (ν_1) (in-plane totally symmetric stretching mode). The extremum of the vibrational motion, in black, is compared to the equilibrium geometry, in gray.

Department of Chemistry, Stanford University, Stanford, CA 94305-5080, USA.

*Present address: Department of Chemistry, Vanderbilt University, Nashville, TN 37235, USA.
†To whom correspondence should be addressed.

1B). An additional photon ionizes the molecule from the electronically excited state. Because the geometry of the Rydberg state is almost the same as that of the ion, the vibrational state prepared in the intermediate state is retained in the ion. With this method, NH_3^+ ions are generated with 80 to 100% efficiency in a single vibrational state that can be just umbrella mode excitation (*14*) or a combination of breathing mode and umbrella mode excitation (*18*).

Reactions are carried out in a guided-ion-beam quadrupole-octopole-quadrupole mass spectrometer, which has been described in detail elsewhere (*19*). A beam of vibrationally excited ions with a controlled kinetic energy passes through a collision region into which the neutral reactant is introduced as a thermalized gas. The collision energy of the reaction is determined by the potential difference between the region in which the ions are formed and where they can react. An octopole ion guide brings the mass-selected reactant ions to the collision region and subsequently directs the unreacted ions and the newly formed product ions to the second quadrupole mass filter. The measured product-ion signals are used to determine the product branching ratios. All product channels are expected to be detected with the same efficiency at the conditions and collision energies in the present work (*19*).

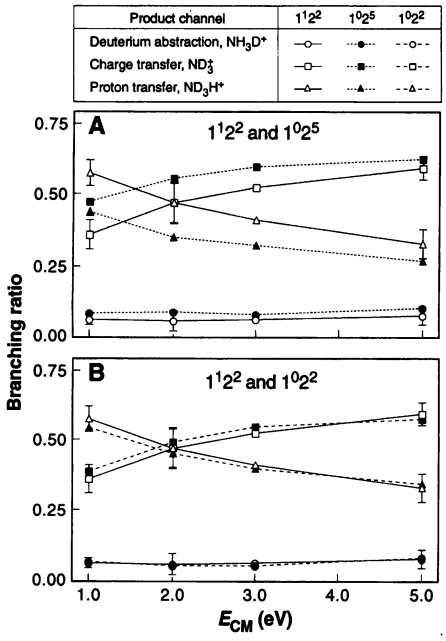

Fig. 2. Product branching ratios for the reaction $NH_3^+(\nu_1, \nu_2) + ND_3$ plotted as a function of center-of-mass collision energy (E_{CM}). (**A**) Comparison of nearly isoenergetic vibrational state preparations of the reagent ion with excitations of $\nu_1 = 1$, $\nu_2 = 2$ (1^12^2) (0.63 eV) and $\nu_1 = 0$, $\nu_2 = 5$ (1^02^5) (0.60 eV). (**B**) Comparison of identical amounts of umbrella bending mode excitation with and without breathing mode excitation: $\nu_1 = 1$, $\nu_2 = 2$ (1^12^2) (0.63 eV) or $\nu_1 = 0$, $\nu_2 = 2$ (1^02^2) (0.24 eV), respectively. Error bars ($\pm 2\sigma$) for the 1^12^2 data are included as representative uncertainties.

We have studied the $NH_3^+ + ND_3$ reaction using multiphoton ionization to prepare the NH_3^+ reagent in two nearly isoenergetic vibrational states. The NH_3^+ reagent is prepared with one quantum of breathing motion and two quanta of the umbrella bending motion (denoted by $\nu_1 = 1$, $\nu_2 = 2$ or 1^12^2) at a total internal energy of 0.63 eV (*15*, *20*), or it is prepared with no breathing motion and five quanta of the umbrella bending motion (denoted by $\nu_1 = 0$, $\nu_2 = 5$ or 1^02^5) at a total internal energy of 0.60 eV (*20*, *21*). A strong dependence of the product branching ratio of this reaction on the reactant-ion umbrella-mode excitation has been previously observed (*13*, *22*), but the comparative effects of other types of vibrational motions have not been investigated. The excitation of differing vibrational motions in the reagent ion addresses directly the question of whether it is the amount of internal energy that influences the reaction outcome or if the type of vibrational motion can also be a factor.

The product branching ratios as a function of center-of-mass collision energy for the two nearly isoenergetic vibrational levels of the NH_3^+ reagent are presented in Fig. 2A. The proton transfer channel is enhanced for 1^12^2 NH_3^+ excitation relative to 1^02^5 excitation, whereas the other two product channels, deuterium abstraction and charge transfer, are depleted. Given the nearly identical internal energies of the reagent ion, Fig. 2A indicates that this polyatomic ion-molecule reaction is mode selective.

To determine the extent to which the reaction outcome has been affected by the differing umbrella mode excitation in the two state preparations, we compared identical amounts of umbrella mode excitation with ($\nu_1 = 1$, $\nu_2 = 2$ or 1^12^2) and without ($\nu_1 = 0$, $\nu_2 = 2$ or 1^02^2) breathing mode excitation. These preparations correspond to internal energies of 0.63 and 0.24 eV, respectively. Over the collision energy range studied, the breathing mode does not significantly influence the product branching ratio for this reaction system (Fig. 2B). The sensitivity to umbrella motion and the insensitivity to breathing motion is a clear signature of mode selectivity.

In the case of the abstraction reactions of H or Cl with HOD, nearly total control of the product branching ratio was demonstrated, in which either side of the HOD could be made to react almost exclusively. The $NH_3^+ + ND_3$ reaction shows a much more modest degree of control but does provide a glimpse into the complex role that internal energy can play in determining reaction outcome. The three product channels are believed to result from direct mechanisms (*22–24*), which means that the duration of the reactive interactions is less than a rotational period (~1 ps). These brief interactions do not provide sufficient time for the energy of the reacting species to become extensively redistributed. Therefore, sensitivity to the vibrational state of the reactant ion is not unexpected.

The difference between vibrational excitation of the umbrella mode and the breathing mode is more difficult to understand considering the previous work demonstrating the significant role that umbrella mode excitation plays in this reaction system (*13*, *22*, *24–27*). The product branching ratio was sensitive to both collision energy and umbrella mode excitation, with the latter being nearly four times more effective than the former (*13*). These results were rationalized by a reaction model in which vibrational motion along the reaction coordinate enhances reactivity whereas motion perpendicular to the reaction coordinate hinders reactivity or is ineffective. This model successfully explained why umbrella mode motion enhances deuterium abstraction (Eq. 1a) but hinders proton transfer (Eq. 1c). The breathing mode excitation is expected to represent motion along the reaction coordinate of the proton transfer channel. In this context, the relative inactivity of the energetic breathing mode [1 quantum = 0.39 eV (*15*)] is puzzling and requires a theoretical treatment more detailed than the simple consideration of the $NH_3^+ + ND_3$ reaction as the dynamics of three quasi-particles, NH_3 and D-ND_2 (*28*).

REFERENCES AND NOTES

1. M. Kneba and J. Wolfrum, *Annu. Rev. Phys. Chem.* **31**, 47 (1980).
2. F. F. Crim, *ibid.* **35**, 657 (1984).
3. A. Sinha, M. C. Hsiao, F. F. Crim, *J. Chem. Phys.* **92**, 6333 (1990).
4. ———, *ibid.* **94**, 4928 (1991).
5. M. J. Bronikowski, W. R. Simpson, B. Girard, R. N. Zare, *ibid.* **95**, 8647 (1991).
6. M. J. Bronikowski, W. R. Simpson, R. N. Zare, *J. Phys. Chem.* **97**, 2194 (1993).
7. A. Sinha, J. D. Thoemke, F. F. Crim, *J. Chem. Phys.* **96**, 372 (1992).
8. G. C. Schatz, M. C. Colton, J. L. Grant, *J. Phys. Chem.* **88**, 2971 (1984).
9. Previous work by Anderson and co-workers showed that internal excitation of a polyatomic ion can affect the product branching of ion-molecule reactions. See, for example, B. Yang, Y. Chiu, S. L. Anderson, *J. Chem. Phys.* **94**, 6459 (1991); T. M. Orlando, Y. Baorui, S. L. Anderson, *ibid.* **90**, 1577 (1989); T. M. Orlando, B. Yang, Y.-H. Chuim, S. L. Anderson, *ibid.* **92**, 7356 (1990).
10. K. Ravichandran, R. Williams, and T. R. Fletcher [*Chem. Phys. Lett.* **217**, 375 (1994)] have also demonstrated that vibrational excitation of a neutral polyatomic reagent affects the rate of reaction with a neutral diatom.
11. W. L. Hase and Y. J. Cho, *J. Chem. Phys.* **98**, 8626 (1993).
12. S. Chapman and D. L. Bunker, *ibid.* **62**, 2890 (1975).

13. L. A. Posey, R. D. Guettler, N. J. Kirchner, R. N. Zare, *ibid.* **101**, 3772 (1994).
14. W. E. Conaway, R. J. S. Morrison, R. N. Zare, *Chem. Phys. Lett.* **113**, 429 (1985).
15. P. J. Miller, S. D. Colson, W. A. Chupka, *ibid.* **145**, 183 (1988).
16. M. N. R. Ashfold, C. L. Bennett, R. J. Stickland, *Comments At. Mol. Phys.* **19**, 181 (1987).
17. W. R. Harshbarger, *J. Chem. Phys.* **53**, 903 (1970).
18. D. J. Leahy and R. N. Zare, unpublished data.
19. R. D. Guettler *et al.*, *J. Chem. Phys.* **101**, 3763 (1994).
20. J. H. Glownia, S. J. Riley, S. D. Colson, J. C. Miller, R. N. Compton, *ibid.* **77**, 68 (1982).
21. J. B. Pallix and S. D. Colson, *J. Phys. Chem.* **90**, 1499 (1986).
22. S. Tomoda, S. Suzuki, I. Koyano, *J. Chem. Phys.* **89**, 7268 (1988).
23. W. J. Chesnavich and M. T. Bowers, *Chem. Phys. Lett.* **52**, 179 (1977).
24. W. E. Conaway, T. Ebata, R. N. Zare, *J. Chem. Phys.* **87**, 3453 (1987).
25. W. A. Chupka and M. E. Russell, *ibid.* **48**, 1527 (1968).
26. T. Baer and P. T. Murray, *ibid.* **75**, 4477 (1981).
27. D. V. Pijkeren, E. Boltjes, J. V. Eck, A. Niehaus, *Chem. Phys.* **91**, 293 (1984).
28. H. Tachikawa and S. Tomoda, *ibid.* **182**, 185 (1994).
29. L.A.P. was supported by an NSF Postdoctoral Research Fellowship in Chemistry (CHE-89-07493). Financial support also came from the Air Force Office of Scientific Research (F49620-92-J-0074).

24 June 1994; accepted 2 August 1994

Spring Phytoplankton Production in the Western Ross Sea

Kevin R. Arrigo* and Charles R. McClain

Coastal zone color scanner (CZCS) imagery of the western Ross Sea revealed the presence of an intense phytoplankton bloom covering >106,000 square kilometers in early December 1978. This bloom developed inside the Ross Sea polynya, within 2 weeks of initial polynya formation in late November. Primary productivity calculated from December imagery (3.9 grams of carbon per square meter per day) was up to four times the values measured during in situ studies in mid-January to February 1979. Inclusion of this early season production yields a spring-to-summer estimate of 141 to 171 grams of carbon per square meter, three to four times the values previously reported for the western Ross Sea.

In the western Ross Sea (Fig. 1), a large polynya forms north of the Ross Ice Shelf in late spring. The availability of light and nutrients within this polynya favors algal growth, and blooms of phytoplankton (pigment >1 mg m^{-3}) have been observed there in mid-January and later (*1*–*6*). In situ oceanographic data rarely have been collected in the Ross Sea before this time of year because heavy sea ice cover prevents ship access to the polynya during austral spring (October through December). In this report, we use data from the CZCS and the scanning multi-channel microwave radiometer (SMMR) to evaluate distributions of algal pigments and sea ice in the western Ross Sea and the Ross Sea polynya.

We processed a time series of six CZCS images (see the legend of Fig. 2) of phytoplankton pigment and sea ice distribution (using the 750-nm channel) within the western Ross Sea (Table 1), which were obtained during the austral spring and summer of 1978–79 between 10 December and 19 February. Lower resolution (30-km) images of sea ice cover from the SMMR also were processed (*7*) for the Southern Ocean for 1978–79. The Ross Sea polynya was first visible in SMMR imagery on 25 November 1978 and continued to increase in size until 6 January 1979 when it became contiguous with the rest of the Ross Sea.

The earliest springtime CZCS image (10 December) revealed the presence of an intense phytoplankton bloom located south of 75°S. Pigment concentrations estimated at 10 to 40 mg m^{-3} covered an area of ~106,000 km^2 (Fig. 2A). By 23 December, the western margin of annual sea ice had receded westward and a dense phytoplankton bloom had developed near the retreating ice edge between 73° and 75°S, increasing the size of the high-pigment (≥10 mg m^{-3}) region to >126,000 km^2 (Fig. 2B).

The CZCS image for 5 January (Fig. 2C), although contaminated by clouds, revealed that the area of high pigments had diminished substantially and that the phytoplankton bloom was in a state of decline. By 16 January, pigment concentrations over much of the region had dropped to 0.2 to 2.0 mg m^{-3} (Fig. 2D). The most coherent bloom was located in Terra Nova Bay (75°S, 166°E), where pigment concentrations ≥10 mg m^{-3} covered an area of >8000 km^2. Patches of enhanced pigments (1.0 to 12 mg m^{-3}) were also apparent south of 76°S. The 25 January image (Fig. 2E) was similar to that of 16 January, except that the bloom in Terra Nova Bay was more extensive (~16,000 km^2).

By 19 February, the phytoplankton bloom in the western Ross Sea had declined further, both in area and in pigment concentration (Fig. 2F). Pigments over most of the western Ross Sea were reduced to <1 mg m^{-3}. Only near the western coast and along the Ross Ice Shelf were pigment concentrations greater than 2 mg m^{-3}.

The distribution and magnitude of pigments shown in images from 16 January and later agree well with the results of field studies undertaken at the same time of year (*4*–*6*). Like the CZCS studies, these studies observed waters with low chlorophyll a content north of 75°S and pigment concentrations ranging from 2 to 7 mg m^{-3} southward to the Ross Ice Shelf. This agreement, along with results from validation studies of CZCS for the Southern Ocean (*8*), strongly imply that our estimates of pigment concentration in the Ross Sea are reliable.

Table 1. Seasonal change in CZCS-derived pigment concentration and primary production in the western Ross Sea. Primary production was calculated for each valid pixel according to the regression model of Eppley *et al.* (*12*) and averaged for the full scenes shown in Fig. 2. This model is based on an empirical relation between the mean pigment concentration in the top optical depth and the rate of primary production in situ. It does not require knowledge of the euphotic or mixed layer depth. Rates of primary productivity calculated by this regression, which includes data from the Arctic Ocean and the Southern Ocean, show good agreement with in situ rates of primary production in the western Ross Sea. For example, in situ studies of waters containing 1.5 to 8.2 mg of chlorophyll a per cubic meter measured an average primary productivity rate of 1.4 g of carbon per square meter per day, with values approaching 2 g of carbon per square meter per day (*5*). At similar pigment concentrations, the method of Eppley *et al.* (*12*) yields a production rate of 1.2 to 2.8 g of carbon per square meter per day.

Date	Mean pigment (mg m^{-3} ± SD)	Cloud-free pixels (%)	Pixels >10 mg m^{-3} (%)	Mean production (g C m^{-2} day^{-1} ± SD)
10 Dec. 1978	22.6 ± 19.3	75.9	61.0	3.90 ± 2.72
25 Dec. 1978	12.7 ± 17.1	66.5	36.7	2.54 ± 2.50
5 Jan. 1979	12.5 ± 16.0	34.2	40.4	2.66 ± 2.34
16 Jan. 1979	1.65 ± 3.24	84.7	1.14	0.99 ± 0.82
25 Jan. 1979	3.57 ± 7.45	82.1	12.2	1.32 ± 1.35
19 Feb. 1979	4.07 ± 11.0	46.1	10.5	1.19 ± 1.63
Spring-summer production (10 Dec. to 19 Feb.)				141 g C m^{-2}

National Aeronautics and Space Administration, Goddard Space Flight Center, Greenbelt, MD 20771, USA.

*To whom correspondence should be addressed.